Two populations of the solar magnetic field

V.N. Obridko[1⋆], I.M. Livshits[1], D.D. Sokoloff[1,2],
[1] *IZMIRAN, 4 Kaluzhskoe Shosse, Troitsk, Moscow, 142190, Russia*
[2] *Department of Physics, Moscow state University, Moscow, 119991, Russia*

Received ..... ; accepted .....

ABSTRACT
Dynamo theory suggests that there are two types of solar dynamo, namely the conventional mean-field dynamo, which produces large- and small-scale magnetic fields involved in the activity cycle and also the small-scale dynamo which produces a cycle independent small-scale magnetic field. The relative contribution of the two mechanisms to solar magnetism remains a matter of scientific debate, which includes the opinion that the contribution of the small-scale dynamo is negligible. Here we consider several tracers of magnetic activity that separate cycle-dependent contributions to the background solar magnetic field from those that are independent of the cycle. We call background fields the magnetic fields outside active regions and give further development of this concept. The main message of our paper is that background fields include two relative separate populations. The background fields with a strength up to 100 Mx cm^{-2} are very poorly correlated with the sunspot numbers and vary little with the phase of the cycle. In contrast, stronger magnetic fields demonstrate pronounced cyclic behavior. We discuss how this result can be included in the above mentioned concepts of solar dynamo studies.

Key words: Solar activity, solar magnetic field, solar activity cycle

1 INTRODUCTION

The solar magnetic activity cycle considered as a global phenomenon is believed to be driven by a wave of large-scale magnetic field propagating somewhere inside the solar convective shell. In this context, the large-scale magnetic field means a magnetic field of scale more or less comparable with the solar radius. The solar dynamo, which is considered to be a physical process underlying the solar cycle, describes the generation and propagation of the activity wave (which is known in this context as the dynamo wave) to various levels of accuracy. Mean-field dynamo models identify the large-scale magnetic field with the mean magnetic field obtained as a result of magnetic field averaging taken over statistical ensembles of convective cells. It allows us to obtain in various approximations closed equations for the mean magnetic field and the mean velocity of the solar media with coefficients parametrized by various quantities related to small-scale characteristics of magnetic and velocity fields. Historically such a model was suggested by E.Parker (1955). The well-known Babcock-Leighton mechanism can also be considered in the framework of mean-field dynamo models with specific parametrization of dynamo driven parameters (see e.g. Dikpati & Gilman, 2009). Contemporary mean-field dynamo models include various physical processes (e.g., Choudhuri et al., 1995; Kitiashvili & Kosovichev, 2011; Pipin & Kosovichev, 2014; Karak et al., 2015). However these do not involve small-scale magnetic fields in an explicit form. Of course, the role of small-scale contributions is stressed in the course of evaluation of the mean-field equations (e.g., Krause & Rädler, 1980). However this role becomes almost invisible when making comparisons with observational data.

The problem of the participation of small-scale magnetic fields in the solar cycle has an additional important aspect. The point now is that, apart from the large-scale dynamo, which produces large-scale magnetic field *together with* small-scale magnetic field, another dynamo mechanism, the so-called small-scale dynamo, which produces small-scale magnetic field only, may operate. Such a possibility was first emphasized by Batchelor (1950), see details in Zeldovich et al. (1990).

Strictly speaking, separation of two mechanisms for small-scale magnetic field generation is related to the linear stage of dynamo process when action of magnetic force on the flow can be neglected. Of course, magnetic field usually plays a role as a governing factor for the flow. Dynamo action becomes non-linear and two populations of small-scale magnetic fields becomes not fully separated. Coexistence of two populations of small-scale magnetic fields is still not sufficiently addressed in dynamo studies, see, however, Subramanian (1998).

Modern progress in observational techniques gives us a

⋆ obridko@izmiran.ru

rich choice of possibilities to observe small-scale magnetic structures at the solar surface, and it is natural to attempt to understand them as a direct result of small-scale dynamo action at or below the solar surface.

In particular, Sokoloff et al. (2015) suggested an observational test, based on statistics of sunspot groups that do not follow the Hale polarity law, and this supports the viewpoint that a small-scale dynamo is active somewhere in the solar interior and gives a cycle-independent contribution to surface tracers of the solar magnetic field.

Of course, this observational test is far from straightforward and the separation between cycle dependent and cycle independent tracers of small-scale solar magnetic field appears an attractive aim. This is the aim of this paper. At present, there are two databases formed of high-resolution observations carried out with single-type instruments. These are SOHO/MDI and SDO/HMI. Michelson Doppler Imager (MDI) onboard the Solar and Heliospheric Observatory (SOHO) (Scherrer et al., 1995) continuously measured the Doppler velocity, longitudinal magnetic field, and brightness of the Sun for 15 years up to 12 April 2011. The enhanced Helioseismic and Magnetic Imager (HMI: Scherrer et al., 2012; Schou et al., 2012) onboard the Solar Dynamics Observatory (SDO: Pesnell, Thompson,and Chamberlin, 2012) began making its routine observations on 30 April 2010. HMI data include all MDI observables, but with much higher spatial and temporal resolutions and better data quality. The optical resolution of these instruments is comparable and is 1.17 arcsec and 0.91 arcsec for MDI and HMI, respectively. At the same time, the size of pixels differs essentially. In full-disc observations, it is 1.98 arcsec for MDI and almost four times less (0.505 arcsec) for HMI. A careful pixel-by-pixel comparison of the HMI and MDI signals was performed by Liu et.al. (2012). The noise of a single measurement was 10.2 Mx cm^{-2} for the 45-second HMI magnetograms and 26.4 Mx cm^{-2} for the one-minute full-disk MDI magnetograms. The averaging over longer intervals, naturally, somewhat decreases the noise level. The noise in the HMI and MDI line-of-sight magnetic-field synoptic charts appears to be fairly uniform over the entire map. The noise is 2.3 Mx cm^{-2} for HMI charts and 5.0 Mx cm^{-2} for MDI charts. Besides that, the line-of-sight magnetic signal inferred from the calibrated MDI data is greater than that derived from the HMI data by a factor of 1.40.

The analysis of Shibalova et al. (2017) confirms that the distribution of the surface magnetic field is substantially intermittent, and in this sense it supports the idea of the small-scale solar dynamo action. As to the small-scale magnetic field as independent component of the total solar magnetic field, we believe that the situation here is more delicate. Indeed, some quantities related to the fractal small-scale magnetic field structure, in particular are almost cycle-independent. The other quantity, the dependence of the field strength on the space scale, demonstrates a cyclic behavior. Perhaps, both excitation mechanisms, i.e. the mean-field and small scale dynamos, are two extreme cases of a general dynamo process, which is active in a wide range of scales.

Our analysis of the cyclic variation of magnetic fields of different strengths requires long-term uniform and homogeneous observations. Therefore, we will first discuss the results based on MDI data and, then, carry out a similar analysis of HMI data.

Comparative analysis of data obtained with various instruments is a natural stage of astronomical research; however it is coherent with the spirit of small-scale dynamo studies as well. The point is that each instrument preforms a specific averaging of physical quantities of interest, while theoretical studies (e.g. Zeldovich et al., 1990) tell that the averaged quantities of intermittent magnetic field may substantially depend on the particular type of averaging. Of course, demonstration that a quantity was calculated from the data obtained from various instruments is important in this context.

2 CONCEPT OF BACKGROUND MAGNETIC FIELD

The term "background magnetic field" initially referred to the solar magnetic field outside active regions containing strong local fields. The wording implicitly implied that statistical properties of the background field depend weakly on time and spatial coordinate, and the main problem was thought to be the definition of the boundaries of the active regions, which were traditionally identified with the 20 Mx cm^{-2} isoline. Much the same meaning is associated with "basal magnetic field" Stenflo (2012).

Modern progress in high resolution solar observations demonstrates that the above informal understanding requires substantial improvement. The point is that the magnetic field outside active regions can vary sharply on the scale of $2''$ and below in magnitude, and even in sign. Figure 1a shows the longitudinal magnetic field of the Sun as obtained from SOHO/MDI on November 27, 1999. The optical resolution of the telescope is $1.17''$, the pixel size is $1.98''$ (Schou et al., 2012). Figure 1b represents the absolute (i.e., unsigned) values of the longitudinal (line-of-sight) field. It can be seen that the field is strongly variable both in sign and in magnitude, depending on the spatial coordinates.

In order to quantify this sharp magnetic field variability Ivanov & Obridko (2002); Obridko & Shelting (2011) introduced the unipolarity index (IU), defined as the ratio of the absolute value of the mean latitudinal magnetic field B_L to its mean absolute value:

$$IU = | < B_L > |/ < |B_L| > \ . \qquad (1)$$

For a strictly unipolar field, $IU = 1.0$, while in the regions of mixed polarity, this value is close to zero.

For the magnetic field shown in Fig. 1a,b the unipolarity index is given in panel Fig. 1c. It can be seen that its value does not exceed 0.3 over most of the disc. The majority of the flux of the small elements of the background field closes in the immediate vicinity of the elements.

The flux of the background field is larger than that of the local fields (i.e. the fields in sunspots/active regions). The total magnetic flux of sunspots changes by a factor of 10-12 during an 11-year cycle, whereas the flux of the large-scale fields changes by less than a factor 2, and the total magnetic flux of sunspots does not exceed 11-14% of the total magnetic flux of the Sun (Harvey, 1996).

Thus, a characteristic feature of the background fields is their small spatial scale. Apparently, they form a special

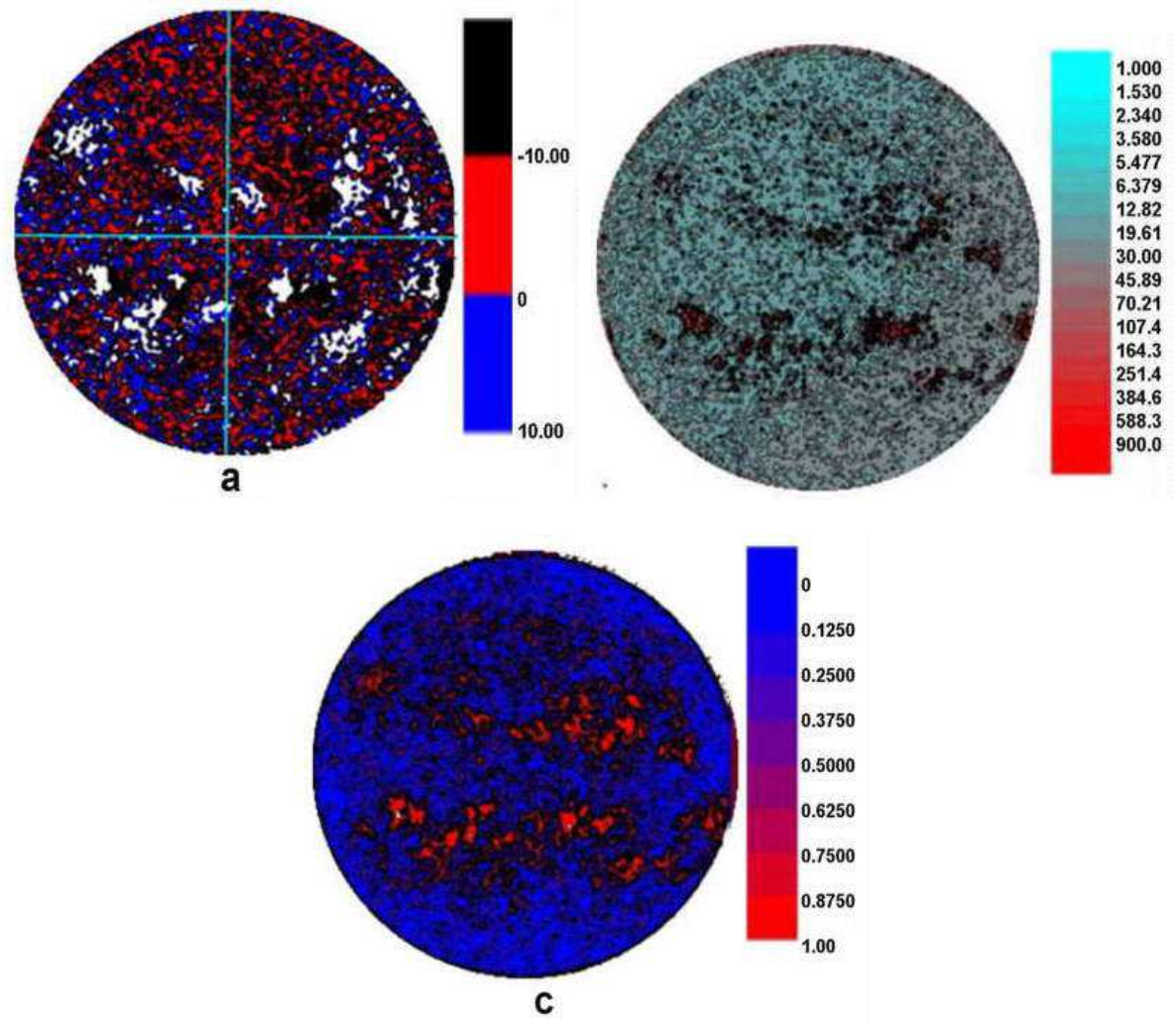

Figure 1. Magnetic field of the Sun at a resolution of 2″ as obtained from SOHO/MDI November 27, 1999: a - longitudinal field, b - absolute value of the longitudinal field, c - unipolarity index. Magnetic field in Figs. 1a and 1b is given in units Mx cm^{-2}. The white areas in Fig. 1a are the areas where the flux in pixels is > 10 Mx cm^{-2}.

population, which obeys its own specific laws of cyclic variation, and the background magnetic fields are the objects with the lowest field values. However, specifying their characteristics is quite a challenge because of their low intensity and small characteristic dimensions.

3 BACKGROUND MAGNETIC-FIELD INTENSITY VERSUS RESOLUTION

In this study we are going to determine the variation of small-scale fields in the course of an activity cycle. Our first task is to clarify how the background magnetic field intensity scales with resolution. We use SOHO/MDI data ($http://soi.stanford.edu//magnetic/index5.html$) for 15 years from 1996 to 2010. So, the data covered the period from the minimum between cycles 22 and 23 up to the beginning of the rise phase of cycle 24. In each year, we chose for investigation some periods of length not less than 27 days. The total number of the magnetograms analyzed was 393. On each day, one 30-second full-disc magnetogram of the longitudinal field is used (usually it is the first of the 16 magnetograms obtained on a given day). MDI provides a full-disc image in the field of view of 34×34 arc min. The image is based on a matrix of 1024×1024 pixels. Thus, the effective field of view of each pixel is 2″. The sensitivity of the magnetograph is about 20 Mx cm^{-2} (Scherrer et al., 1995).

The observed structure of the magnetic field is highly dependent on the resolution. As the effective observational window increases (the resolution decreases), the contribution of elements with mutually opposite signs is cancelled. This can be simulated by numerical smoothing.

Pietarila Graham et al. (2009) and Stenflo (2011) show that such a smoothing makes the mean field decrease as D^{-k}. Stenflo (2011) obtained $k = 0.13$, and Pietarila Graham et al. (2009) reported a somewhat larger value $k = 0.26$. In any case, the values of k obtained are much smaller than unity, which corresponds to the random noise distribution. This means that the elements of the weak field do not arise as a result of a random process, but reflect a process, which can be compared with the small-scale dynamo. Shibalova et

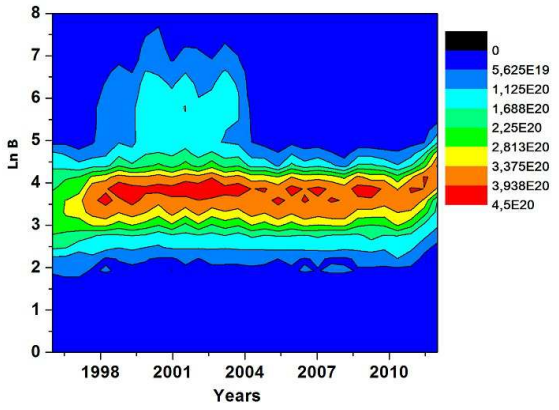

Figure 2. Contributions of magnetic fields of different scales to the total magnetic flux for each Carrington rotation. Magnetic field is measured in Mx cm^{-2}, magnetic flux is measured in Mx (colour scale).

al. (2017) have shown that k changes from unity at the cycle minimum to very small values at the maximum, thus reflecting gradual changes in the contribution of small-scale fields and active regions. The mean for a cycle is 0.30, which is close to the value obtained by Pietarila Graham et al. (2009).

4 CONTRIBUTION OF MAGNETIC FIELDS OF DIFFERENT INTENSITY TO THE INTEGRAL MAGNETIC FLUX AS INFERRED FROM SOHO/MDI DATA

Our next aim is to identify the relative contributions of magnetic fields of different scales. We summed the absolute values of the field in the range from 1 Mx cm^{-2} to 3000 Mx cm^{-2} or, in terms of the natural logarithm values, from 0 to 8. The summation was performed using a step $\Delta \ln B = 0.1$. Fig. 2 shows this distribution, which is in fact a two-dimensional field spectrum. Fig. 2 represents the magnetic flux for fields of different intensity B. For each value of $\ln B$ in the range from 0.05 to 7.95, we found such boundary values $B1$ and $B2$ that $\ln B1 = \ln B - 0.05$ and $\ln B2 = \ln B + 0.05$. Then, we calculated the sum of unsigned flux values in all pixels where B ranges from $B1$ to $B2$. The color scale shows the flux values in units 10^{20} Mx.

We see from Fig. 2 that the main contribution to the magnetic flux comes from the range $\ln B = 3.5$ (i.e., $B \approx 33$ Mx cm^{-2}) and that this contribution is almost time independent. Of course this value is fairly close to the noise level of the SOHO/MDI magnetograph (20 Mx cm^{-2}, Sherrer et al., 1995); however we note that the entire contribution to the magnetic flux from the range of fields up to 100 Mx cm^{-2} is almost time independent.

We note, however, a detail in the vicinity of the year 2000 where the contribution from fields stronger than 250 Mx cm^{-2} (250 Mx cm^{-2} corresponds to $dB \approx 5$) increases slightly. However it still remains much smaller than the contribution of the 33 Mx cm^{-2} field.

Our next objective is to separate the contributions to the small-scale field that are associated with sunspots and those that are sunspot independent. To this end, we summed the absolute field values for 393 days in cycle 23 (1996-2010) in the pixels if those values did not exceed 33, 100, and 3000 Mx cm^{-2}, and plotted this sum vs. the daily sunspot numbers on the same observation days (Fig. 3). We see from this figure that the contribution to the magnetic flux that comes from weak magnetic fields (< 33 Mx cm^{-2} and < 100 Mx cm^{-2}) is almost independent of the phase of the cycle. In contrast, the contribution to the flux coming from fields that do not exceed 3000 Mx cm^{-2} (that is the total flux)is clearly connected with the phase of activity cycle. The contribution of fields < 100 Mx cm^{-2} determines almost 100% of the total magnetic flux at the minimum of the cycle (2008-2010) and only about 50% at the maximum (2000-2002).

The relative areas occupied by the magnetic fields of intensity < 100 Mx cm^{-2} are, respectively, 99.3% at the minimum and 94.4% at the maximum of the cycle (see Fig. 3, right panel; to save space we do not give other plots of this type). The mean intensity of the fields smaller than 33 Mx cm^{-2} is 15.9 Mx cm^{-2} in the intervals of very low activity and 18 Mx cm^{-2} in the intervals of high activity. The mean value of the fields smaller than 100 Mx cm^{-2} is 18 Mx cm^{-2} at times of both high and low activity. Stronger fields correlate well with the sunspot numbers. Thus, we can conclude that there are two populations of magnetic fields. The weak fields of magnitude less than 33 Mx cm^{-2} and 100 Mx cm^{-2} apparently arise as a result of a small-scale subsurface process, while the stronger fields are connected with the cycle and are generated by the classical mean-field solar dynamo.

Finally, we plot the accumulated flux as a function of a certain limiting field B (Fig. 4). As above, the absolute values of the magnetic field are summarized, and we consider the pixels only where the field is below a certain limit B. Separate calculations are performed for the epochs of minimum (2008-2010, 115 full-disc magnetograms) and maximum (2000-2002, 81 full-disc magnetograms). As a result, we find that there are specific relations for the epochs of the minimum and maximum of the cycle. For fields of about 70 Mx cm^{-2}, the accumulated flux curves are more or less independent on the cycle phase. In contrast, for stronger fields ($\ln B > 4.25$), the magnetic flux at the maximum is much larger than at the minimum.

The total flux is strongly correlated with sunspot numbers; however this correlation is associated with a strengthening of the local magnetic field. The total flux at the point SSN=0 is only 30-40% smaller than at the point SSN=200. This gives a hint that there is a special mechanism, which enhances the field and controls the fields of active regions (i.e., the fields of sunspots and faculae). Although the fields here are much stronger (from 40 Mx cm^{-2} up to 3000 Mx cm^{-2}), their contribution to the total flux is not large (30-40%). These fields are extremely variable; they can change by 10-30% over one or two days.

5 ANALYSIS OF HMI DATA

In this Section, we continue to analyze variations in the integral flux of magnetic fields of different strengths on the basis of HMI data. The calculation method is the same as in the previous Section. However, we had to make some changes to the calculation method. With a relatively moderate resolu-

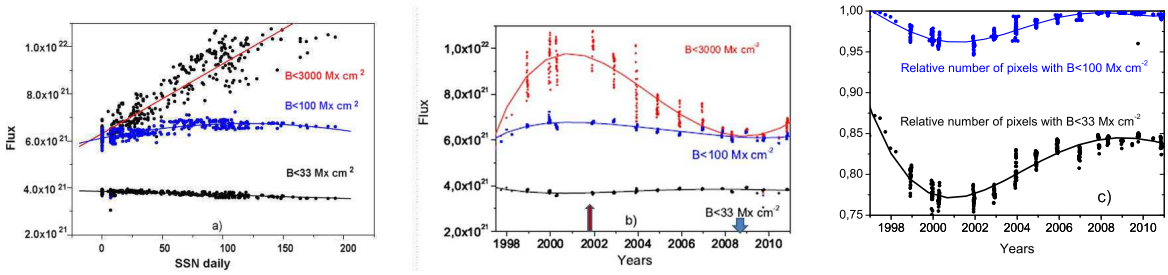

Figure 3. Contributions to magnetic flux (in Mx) coming from magnetic fields which to not exceed the values of 33, 100 and 3000 Mx cm^{-2}, respectively, versus sunspot number on the same day (SSN daily), (left panel), and versus time (middle panel). Data are shown by points and the corresponding trends are given by solid lines. The right panel shows the relative area of the disc occupied by magnetic field weaker than 100 Mx cm^{-2} and weaker than 33 Mx cm^{-2} versus time. Vertical red and blue arrows at the middle panel indicates epochs of solar activity minimum and maximum correspondingly.

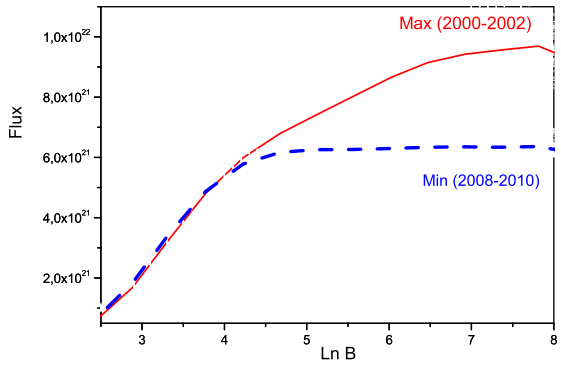

Figure 4. Accumulated magnetic flux (Mx) versus the fields below the limiting value B for solar maximum (solid line) and solar minimum (dashed line).

tion of MDI and a high noise level, we calculated the total flux of the magnetic-field longitudinal component from the entire disk and its variation with the phase of the cycle. Now, with a much higher resolution of HMI and a significantly lower noise level (See Liu et al., 2012), we are going to study more subtle effects associated with the variation of very weak fields. However, in this case it is necessary to take into account that the use of the longitudinal component alone in the analysis of small scales and weak fields may introduce additional errors. Therefore, we have imposed some additional restrictions. The main differences are as follows:

A) The calculations were performed for all days of observation without gaps (i.e., 2226 days). The data were then averaged over 30 days. This makes the time resolution of the new figures more uniform.

B) The flux was not calculated over the entire disk, but only over a central circle of radius $R < 0.7R_{\odot}$ (i.e., the position angle was $\theta < 45°$).

C) All data were divided by $\cos\theta$ to decrease the possible projection effect.

D) A correction was introduced for the change of diameter of the visible solar disk due to the Earth's orbital motion.

E) The flux values are given in units 10^{22} Mx.

Figure 5 illustrates the calculation results in the same format as Figure 3.

One can see that HMI observations reveal the same type of dependence of the magnetic fields on the phase of cycle and sunspot numbers as MDI data. As before, the dependence is poorly pronounced for the fields of strength smaller than 100 Mx cm^{-2} and is almost absent for the fields smaller than 33 Mx cm^{-2}. As in the case of MDI data, the fields smaller than 33 Mx cm^{-2} and smaller than 100 Mx cm^{-2} occupy the majority of the disc area.

There is one more interesting feature in the figure. The total flux has a boundary defined by the number of sunspots. For each sunspot number it is possible to specify the minimum flux value. It is hard to say whether this is a physical limitation, or is simply an artefact of the observation and analysis procedure.

6 CYCLIC VARIATION OF WEAK FIELDS

As mentioned above, the cyclic variation of weak fields is poorly pronounced. Strictly speaking, it is necessary to take into account the possible impact of the magnetograph noise, which, naturally, does not change with the phase of the cycle. Although the noise of a single HMI measurement is 10.2 Mx cm^{-2}, i.e., is far from the boundary value of 100 Mx cm^{-2}, it may nevertheless affect the estimate of the flux of fields smaller than 33 Mx cm^{-2}. This is hardly seen in Fig. 5 where the flux values are given in one and the same scale.

Our calculations show, that the total magnetic flux and the flux $<$ 100 Mx cm^{-2} change in a similar way and display a high correlation. However, the the maximum of the total flux is 2.1 times the minimum of the total flux and the maximum flux for fields $<$ 100 Mx cm^{-2} is 1.2 times larger than the minimum for fields $<$ 100 Mx cm^{-2}. The flux of fields $<$ 33 Mx cm^{-2} is almost uncorrelated with the phase of the cycle and increases toward the end of the observation period only by 3%. Taking into account that the flux of fields $<$ 100 Mx cm^{-2} includes that of $<$ 33 Mx cm^{-2}, it can be stated that the magnetic flux in the entire range of 33-100 Mx cm^{-2} also changes approximately by a factor of 2.

In Fig. 6 we plot our data selecting the appropriate scale for every range. The cycle dependence of the magnetic flux is evident even for weak fields. Note that the flux of weak fields B $<$ 33 Mx cm^{-2} is greater than the flux of

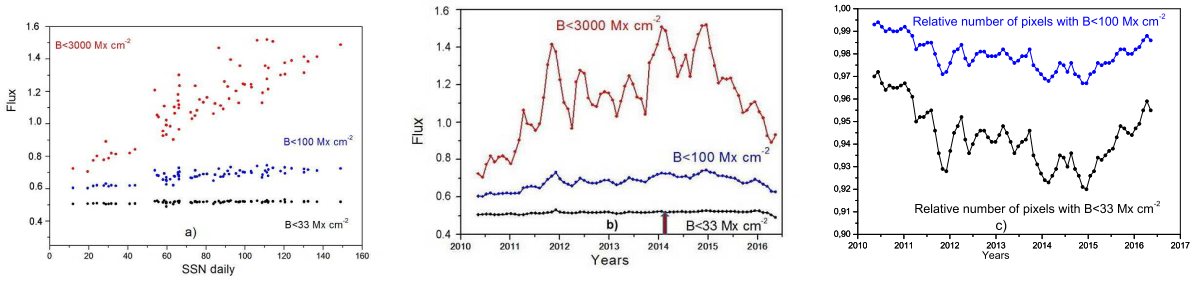

Figure 5. Contributions to magnetic flux (in Mx) coming from magnetic fields, which to not exceed the values of 33, 100 and 3000 Mx cm^{-2}, respectively, versus the sunspot number on the same day (SSN daily), (left panel), and versus time (middle panel). Data are shown by points and the corresponding trends are given by solid lines. The fluxes are given in units 10^{22} mX. The right panel shows the relative area of the disc occupied by magnetic field weaker than 100 Mx cm^{-2} and weaker than 33 Mx cm^{-2} versus time. Red arrow at the middle panel indicates the epoch of solar maximum.

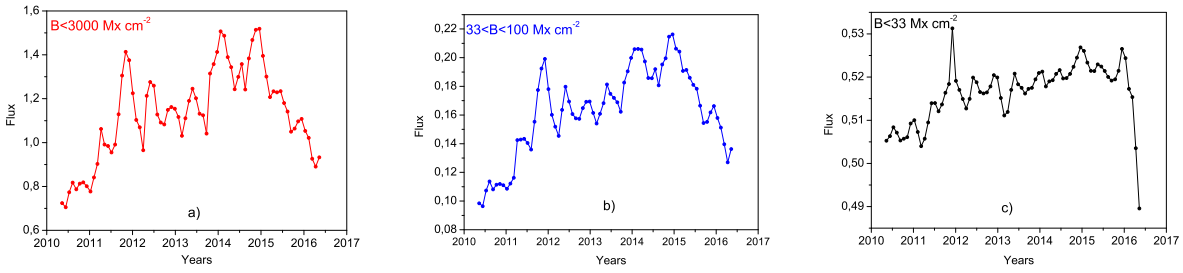

Figure 6. Cyclic variation of fluxes with various strength limits (left $B < 3000$ Mx cm^{-2}, middle $33 < B < 100$ Mx cm^{-2}, right $B < 33$ Mx cm^{-2}). The fluxes are given in units 10^{22} mX.

moderate fields $33 < B < 100$ Mx cm^{-2}. Apparently this is due to the fact that the area of weak fields is very large, and the area variations may disguise intensity variations in the particular pixels when the integral flux is calculated. Therefore, it seems worth examining how the mean field value in these ranges would change per pixel.

7 COLLECTIVE EFFECT IN THE DISTRIBUTION OF WEAK FIELDS

Figure 7 shows the mean field values per pixel for the fields less than 3, 10, 33, and 100 Mx cm^{-2}. The fields less than 3 and 10 Mx cm^{-2} seem to be determined mainly by the instrumental noise and are virtually not associated with the cycle. A slight increase by the end of the time interval under consideration may be an instrumental effect, but it may also be due to a gradual increase in activity by that time. Beginning with the fields < 33 Mx cm^{-2} the cycle dependence is doubtless.

Thus, the dynamo mechanism works beginning with the weakest fields close to the noise limit. However, the picture is more complicated. Both the mean intensity per unit area and the relative area occupied by the fields of different intensities change in the course of a cycle. One process gradually increases the mean field intensity with the approach to the cycle maximum, while the other simultaneously changes the relative area occupied by the fields of different intensities. Therefore, the flux of the weak fields does not depend on the phase of the cycle, but the intensity per unit area does depend.

Figure 8 represents the mean magnetic field in isolated (at least one adjacent pixel has the sign opposite to the pixel under examination), simply non-isolated (all four adjacent pixels have the same sign), and non-isolated25 (all 24 adjacent pixels have the same sign) pixels. One can see that the isolated pixels have very weak field and, in general, behave much like the noise features limited to 3 and 10 Mx cm^{-2} (Figures 7a and 7b). In the pixels surrounded by other pixels of the same sign, the field increases dramatically and even exceeds the mean disc field.

Figure 9 shows the relative area occupied by the pixels of these three types on the disc. The relative area of the isolated pixels is virtually independent of time. The pixels surrounded by four pixels of the same sign form quite a large population and (most significantly) actually coincide with the solar activity curve. The pixels surrounded by 24 pixels of the same sign display approximately the same time dependence, but they are somewhat less frequent.

Thus, the dynamo mechanism contains a mode that increases the magnetic-field intensity per pixel in a group of pixels of one sign.

8 CONCLUSION AND DISCUSSION

The main message of our paper is that background fields include two relative separate populations. The background

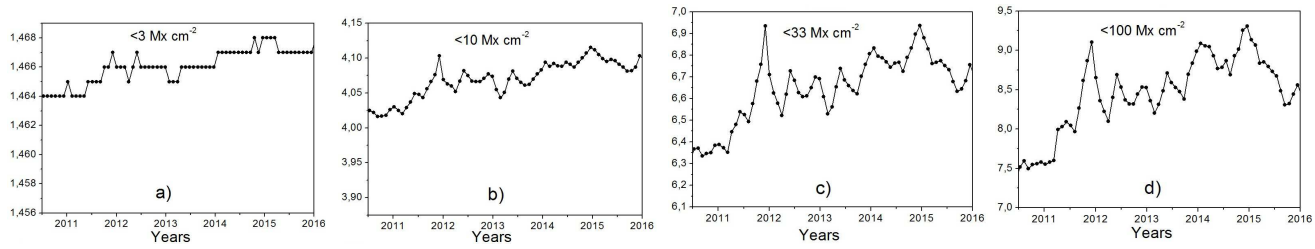

Figure 7. The mean field per pixel in units Mx cm^{-2} for the fields (panels from left to right) less than 3, 10, 33, and 100 Mx cm^{-2}.

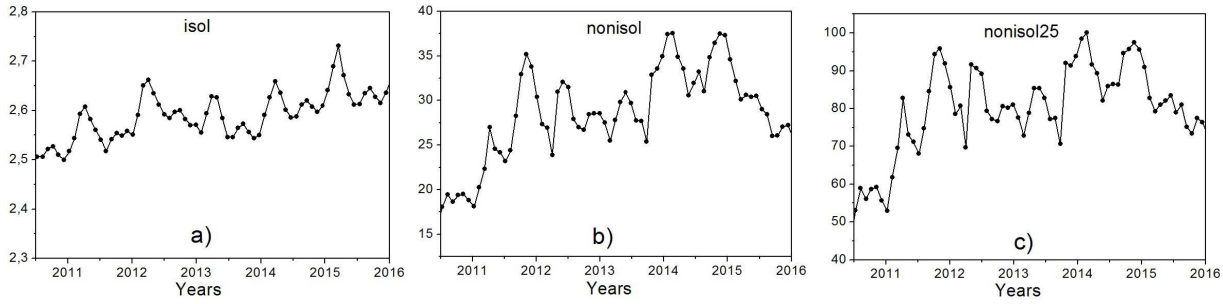

Figure 8. The mean magnetic field in units Mx cm^{-2} in isolated (at least one adjacent pixel has the sign opposite to the pixel under examination, panel a), simply non-isolated (all four adjacent pixels have the same sign, panel b), and non-isolated25 (all 24 adjacent pixels have the same sign, panel c) pixels.

fields with a strength up to 100 Mx cm^{-2} are very poorly correlated with the sunspot numbers and vary little with the phase of the cycle. In contrast, stronger magnetic fields demonstrate pronounced cyclic behavior.

Our main result agrees with a similar conclusion of Jin & Wang (2011) obtained from Hinode observations. Using the Hinode spectropolarimeter data, Buehler et al. (2013), Jin & Wang (2015a) and Jin & Wang (2015b) demonstrated that in the period from 2006 to 2015 the background magnetic field at the centre of the disc changed little. Later on, this result was corroborated for a wider range of latitudes (Lites et al., 2014). Kleint et al. (2010) and Bianda et al. (2014) arrived at the same conclusion when analyzing the Hanle effect for the period from 2007 to 2009.

All these facts apparently mean that the background fields do not arise as a result of the diffusion of active regions, but are the manifestation of a small-scale mechanism. So far, it is unclear whether this is a real mechanism of field generation (a kind of a small-scale dynamo) or it is purely a result of small-scale turbulence.

The concept of the solar small-scale dynamo has been advocated by many authors, e.g. Petrovay & Szakaly (1993), Cattaneo (1999), Lin & Rimmele (1999), Khomenko et al. (2003), Lites et al. (2008), Jin et al. (2009), Lites (2011), see also Jin & Wang (2015a), Borrero et al. (2015) for reviews. The small-scale dynamo as a mechanism of magnetic field self-excitation does not depend on the large-scale dynamo, which generates the global magnetic field of the solar cycle. It looks plausible that this mechanism is determined by twisting and compression of field lines under the influence of turbulent processes. It is not clear whether this small-scale dynamo is distributed throughout the convection zone or is confined to the subsurface layers. More about the general theoretical background for the above studies is given in Sect. 1.

Thus, from the very beginning of the cycle, the entire surface of the Sun is covered with weak fields of intensity from 33 to 100 Mx cm^{-2}. They yield the main contribution to the integral flux both at the minimum and at the maximum of the cycle (Fig. 2). At the minimum, the accumulated flux remains equal to that of fields $\leqslant$ 100 Mx cm^{-2}, since the fields $\geqslant$ 100 Mx cm^{-2} are virtually absent (Fig.4). As the cycle evolves, the area of relatively weak fields somewhat decreases at the expense of sunspots with strong fields (Fig. 3c and Fig. 5c). However, even in relatively weak fields, the dynamo continues to work, so that the field flux per pixel somewhat increases (Figs. 7c and 7d) making up for the decrease in area. For the fields $\leqslant$ 33 Mx cm^{-2}, the decrease in area is fully compensated by the increase in mean flux per pixel (partial flux), so that the integral flux for fields $\leqslant$ 33 Mx cm^{-2} changes by less than 3% and, in any case, does not show any cycle dependence (Fig. 6c). For stronger fields $\leqslant$ 100 Mx cm^{-2}, the flux per pixel at the maximum increases much more significantly; therefore, the cycle dependence can be seen the integral (Fig.6b). However, since the integral flux for the fields $\leqslant$ 33 Mx cm^{-2} (Fig 6c) is much larger than for the fields 33 $\leqslant B \leqslant$ 100 Mx cm^{-2}, the integral flux in the range of moderate fields $B \leqslant$ 100 Mx cm^{-2} varies during the cycle by only 15-20%. So, the dynamo almost does not change the relative fraction of the flux associated with moderate fields, making up for the decrease in relative area by an increase in magnetic flux per pixel. At the maximum of the cycle, the flux in some pixels sharply increases by tens of times. This is especially important in cases where several pixels form a unipolar complex. E.g., the partial flux per pixel in a group of 25 pixels of the same polarity is larger than in isolated pixels by a factor of 40 (Fig. 8). As a result, the integral flux in such complexes, i.e., in spots, becomes comparable with the flux in moder-

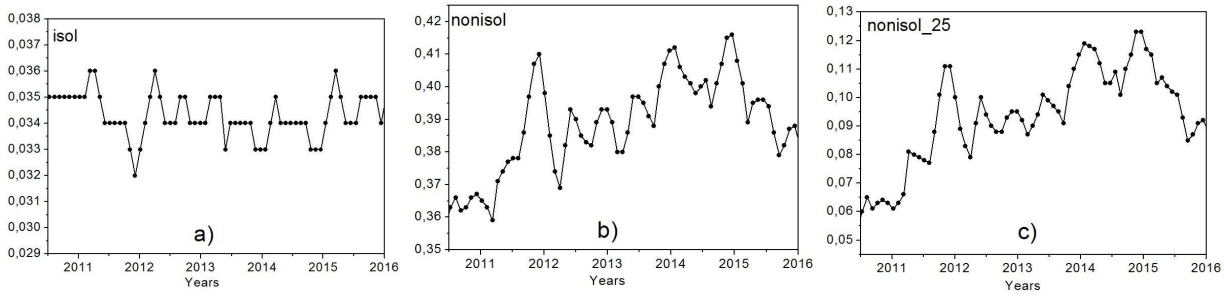

Figure 9. Relative area occupied by the pixels of three types on the disc (notation as in the previous figure).

ate fields, although their area does not exceed 2-3% (Figs. 3c and 5c).

Let us summarize our vision of solar dynamo in light of observations under discussion. The crucial point is to what extent we have to say that there are two solar dynamos which generate two populations of solar magnetic field. In our opinion, it depends on the viewpoint (our interpretation is coherent with ideas of Subramanian, 1998.) If we are going to describe magnetic field in terms of mean quantities, i.e. mean magnetic field, correlation functions etc, we have to say that there are two relatively independent excitation mechanisms, i.e. cyclic mean-field dynamo and non-cyclic small-scale dynamo. If we are going to describe dynamo in context of direct numerical simulations, we have to deal with a unique process which produces two kinds of magnetic field. This activities can be separated spatially or may be attributed to different scales of spectrum. The situation can be compared with well-known corpuscular-wave dualisms: γ-quantum looks more similar as a particle while a radio-wave looks more as a wave while both are two sides of a unique phenomenon.

The relation between the surface diffuse magnetic field and surface magnetic features like sunspots does not directly relate to the scope of tasks of the dynamo studies. Strictly speaking, the dynamo is excited somewhere in the solar interior, and it may happen in principle that small-scale magnetic fields do not penetrate to the surface of a spherical dynamo active body. However it looks more than plausible that magnetic field in the solar interior is already concentrated in magnetic ropes, and this fact is smoothed out in mean-field description. This idea is strongly supported by experiences from various numerical studies as well as theoretical understanding of the problem.

ACKNOWLEDGMENTS

We are grateful to SOHO /MDI and SDO/HMI teams for providing the data used in this research. We are grateful for D.Moss for critical reading of a preliminary version of the manuscript the manuscript. The research is supported by RFBR under grants 17-02-00300 and 15-02-01407.

REFERENCES

Batchelor, G.K., 1950, Proc. R. Soc. Lond., A201, 405
Bianda M., Ramelli R., Gisler D., Stenflo J.O., 2014, in Solar Polarization 7, ed. by K.N. Nagendra, J.O. Stenflo, Q. Qu, M. Samooprna, 167
Borrero J. M., Jafarzadeh S., Schüssler M., Solanki S. K., 2015, Sp. Sci. Rev.,
Buehler D., Lagg A., Solanki S.K., 2013, A&A, 555, 33
Cattaneo F., 1999, ApJ, 515, L39
Choudhuri A.R., Schüssler M., Dikpati M., 1995, A&A, 303, L29
Dikpati M., Gilman P.A., 2009, Sp. Sci. Rev., 144, 67
Golub L., Davis J.M., Krieger A.S., 1979, ApJ, 229, L145
Hagenaar H.J., Schrijver C.J., Title A.M., 2003, ApJ, 584, 1107
Ivanov E.V., Obridko V.N., 2002, Sol. Phys. 206, 1
Ito H., Tsuneta S., Shiota D., Tokumaru M., Fujiki K., 2010, ApJ, 719, 131
Jin C.L., Wang J.X., 2011, ApJ, 732, 4
Jin C.L., Wang J.X., 2015a, ApJ, 806, 174
Jin C.L., Wang J.X., 2015b, ApJ, 807, 70
Jin C.L., Wang J.X., Zhao M., 2009, ApJ, 690, 279
Karak B.B., Kitchatinov L.L., Brandenburg A., 2015, ApJ, 803, 95
Khomenko E.V., Collados M., Solanki S., Lagg A., Trujillo Bueno J., 2003, A&A, 408, 1115
Kitiashvili I.N., Kosovichev A.G., 2011, in The Pulsations of the Sun and the Stars, Lecture Notes in Physics, p. 121
Kleint L., Berdyugina S.V., Shapiro A.I., Bianda M., 2010, A&A, 524, 37
Krause F., Rädler K.-H., 1980, Mean-field magnetohydrodynamics and dynamo theory, Oxford, Pergamon
Lin H.S., Rimmele T., 1999, ApJ, 514, 448
Lites B. W., Kubo M., Socas-Navarro H., Berger T., Frank Z., Shine R., Tarbell T., Title A., Ichimoto K., Katsukawa Y., Tsuneta S., Suematsu Y., Shimizu T., Nagata S., 2008, ApJ, 672, 1237
Lites B.W., 2011, ApJ, 737, 52
Lites B.W., Centeno R., McIntosh S.W., 2014, Publ. Astron. Soc. Jpn., 66, 4
Liu Y., Hoeksema J.T., Scherrer P.H., Schou J., Couvidat S., Bush R.I., Duvall T.L., Jr., Hayashi K., Sun X., Zhao X., 2012, Solar Phys., 279, 295-316.
Livingston W., Harvey J., 1969, Solar Physics, 10, 294
Muller R., Roudier T., 1984, Solar Phys., 94, 33
Obridko V.N., Shelting B. D., 2011, Solar Phys. 270, 297
Parker E.N., 1955, ApJ, 122, 293
Petrovay K., Szakaly G., 1993, A&A, 274, 543
Pietarila Graham, J., Danilovic S., Schüssler M., 2009, ApJ, 693, 1728
Pipin V.V., Kosovichev A.G., 2014, ApJ, 785, 49

Scherrer P.H., Bogart R.S., Bush R.I., Hoeksema J.T., Kosovichev A.G., Schou J., 129, Solar Phys., 1995, 162
Scherrer P.H., Schou J., Bush R.I., Kosovichev A.G., Bogart R.S., Hoeksema J.T., Liu Y., Duvall T.L., Jr., Zhao J., Title A.M., Schrijver C.J., Tarbell T.D., Tomczyk S., 2012, Solar Phys., 275, 207-227.
Schou J., Scherrer P.H., Bush R.I., Wachter R., Couvidat S., Rabello-Soares M.C., Bogart R.S., Hoeksema J.T., Liu Y., Duvall T.L., and 11 coauthors, 2012, Solar Physics, 275, 229-259.
Sheeley N.R., 1966, ApJ, 144, 723
Sheeley N.R., 1967, Solar Phys., 1, 171
Shiota D., Tsuneta S., Shimojo M., Sako N., Orozco Suárez D., Ishikawa R., 2012, ApJ, 753, 157
Shibalova, A.S., Obridko, V.N., Sokoloff, D.D., Solar Phys., 2017, 292, 44
Sokoloff, D., Khlystova, A., Abramenko, V., 2015, MNRAS, 451, 1522
Stenflo J.O., 1982, Solar Phys., 80, 209
Stenflo J.O., 2012, A&A, 547, A93
Subramanian, K., 1998, MNRAS, 294, 718
White O.R., Livingston W.C., 1981, ApJ, 249, 798
Zeldovich Ya.B., Ruzmaikin, A.A. Sokoloff D.D., 1990, The Almighty Chance, World Sciu, Sing.